Evaluation of corrosion damage in reinforced concrete structures in terms of the rebar's residual cross-section

Victor S. Gilayeneh[1,*] and *Sunday* O. Nwaubani[1]

[1]School of Civil and Environmental Engineering, University of the Witwatersrand, Johannesburg, South Africa

Abstract. Corroding reinforced concrete structures are frequently assessed to determine the rate of corrosion propagation and the level of deterioration, which might compromise the structure's reliability. Appropriate measures should be considered in deciding when and how to implement maintenance if safety must be ensured. However, the influential factor that governs or informs such decisions is corrosion damage quantification. Nonetheless, the current non-destructive methods of corrosion damage quantification often lead to ambiguity, and most do not evaluate corrosion damage in terms of the rebar's cross-section loss, which is the primary effect of corrosion. To address these shortcomings, this paper proposes an effective, reliable, and less-complicated model for quantifying corrosion damage in reinforced concrete structures based on the cross-sectional area of the corroding bar. The study was conducted through experimental (laboratory-based) and numerical investigations of the relationship between the level of corrosion and the corrosion-induced crack width. Based on the investigations' findings, appropriate relationships and essential parameters were identified, and the model was derived analytically. The derived model assesses corrosion damage in terms of the corroding bar's residual cross-section and requires only a few input parameters, which can be obtained by non-destructive testing if not known. The model was tested against data obtained from the laboratory experiment and against other experimental and analytical data from the literature, and the results showed a good correlation.

1 Introduction

The maintenance of corroding concrete structures is a challenge to engineers, not only because of the complexity characterising the corrosion process but also the uncertainty of corrosion damage quantification [1,2]. In most instances, these structures are in service, thus, requiring a non-destructive method of evaluation, which often leads to ambiguity. Such situations often lead engineers and practitioners to recommend repair earlier than necessary or when the structure is beyond its limit state. According to Bloomfield [2], if appropriate repairs are to be performed on corrosion-damaged concrete structures, then engineers must fully understand the cause and extent of the damage or risk wasting resources. This implies that appropriate corrosion damage quantification is the most crucial task in the assessment of corroding concrete structures.

Corrosion damage quantification in reinforced concrete structures is one of the areas still underdeveloped and contentious. Although there are some suggested non-destructive models for corrosion damage prediction, the need to adequately quantify the degree of reinforcement corrosion has not been addressed. Most corrosion damage prediction models are imprecise and cannot reproduce the same outcome as the experimental results from which the models were fitted [3], too complicated to be used in real-world conditions [4], and interestingly, most do not evaluate corrosion damage in terms of the rebar's cross-section loss [5].

It must be noted that it is the loss of material from the surface of the corroding bar that leads to a loss in the cross-sectional area and consequently, structural and durability-related issues [6,7]. Thus, the principal impact of corrosion is the reduction in the rebar diameter or bar section, which leads to cracking and spalling of the cover concrete, loss of bonding between the concrete and the embedded steel, and loss of the structure's load-carrying capacity. Several studies, including Zhang et al. [8], Yu et al. [9], and Angst [10], to name a few, have revealed that the cross-section loss reduces both the load-carrying capacity and the bond between the concrete and the rebar. These studies confirmed that Andrade et al. [11] got it right by considering the loss in the rebar section due to corrosion as the fundamental parameter of failure. Therefore, to adequately predict the residual service life (load-bearing capacity and serviceability) of corroding concrete structures, the remaining area of the corroding bar is required.

Despite the ambiguities, inadequacies, and limitations of these damage prediction models, appreciation should be given to their proponents. Their work has set the path for further development towards the quantification of residual life of corrosion-damaged concrete structures. Andrade et al. [11,12] were the first to propose prediction models that linked the loss in load-carrying capacity with the loss of the rebar's diameter. Rodriguez et al. [13] were also the first to establish a linear relationship between the corrosion-induced crack width and the rebar cross-section loss. Studying the amount of corrosion required to

* Corresponding author: victor.gilayeneh1@students.wits.ac.za

generate the first crack, Alonso et al. [14] proposed a model, which for the first time included the depth of the cover concrete as an influencing parameter. Vidal et al. [15] also revealed that the crack width is directly proportional to the volume of oxide produced during the crack propagation phase, which is also proportional to the steel cross-section loss.

Given the above, this paper seeks to address the need for a robust method of quantifying corrosion damage in reinforced concrete structures by proposing an effective, reliable, and less-complicated model. The study was conducted through a laboratory-based experiment and numerical analysis of the relationships between the level of corrosion (cross-section loss and mass loss) and the corrosion-induced crack width.

2 Methods and Procedures

2.1. Laboratory-based Experiment

Among other things, the laboratory-based experiment was conducted to investigate the evolution of the corrosion-induced crack width and its relationship with the rebar's cross-section loss under the influence of chloride-induced corrosion. This experiment consisted of an accelerated corrosion test conducted on five reinforced concrete specimens. All specimens had the dimensions of 500 x 300 x 120 mm, three levels of cover depths, and were reinforced with nine Y10 bars, but with varying compressive and tensile strengths as well as the binder types. Figure 1 and Figure 2 show the cross-section of the laboratory-based specimen and the setup of the impressed current test, respectively.

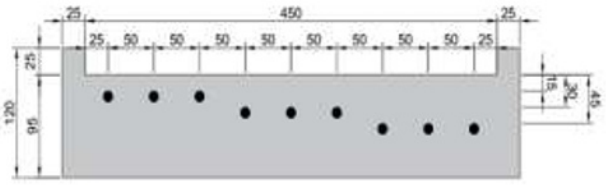

Dimensions in mm

Fig. 1: Cross-section of the Laboratory-based Specimen.

Fig. 2: Setup of the Impressed Current Test.

2.2 Numerical Analysis

The numerical analysis consisted of simulations of steel corrosion in concrete, which were conducted using ANSYS 19.2 workbench student version. The simulations were conducted as plane stress two-dimensional (2D) boundary problems, and this approach was adopted to reduce processing time and improve the accuracy of the results subject to the solver limitation of the student version.

The simulations aimed to structurally predict the behaviours (stresses and deformations) of the system being modelled (steel corrosion in concrete) and study the relationship between the pressure exerted by the expansive corrosion product on the surrounding concrete, which was applied as internal pressure, and the corresponding deformations and resultant stresses. Three cases were considered in this numerical investigation.

Case I was based on the specimens' properties (materials and geometry descriptions) of the laboratory investigation. The compressive strength, tensile strength and concrete density were obtained from the experimental data, while the elastic modulus was deduced from the compressive strength. Figure 3 illustrates the boundary conditions employed in modelling Case I specimens.

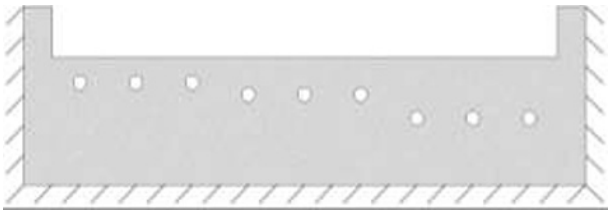

Fig. 3: Boundary Conditions of Case I Specimens.

Case II was arbitrarily selected with material properties of the most used structural concrete to serve as the parametric study. This case also considered five specimens, singly reinforced concrete beams, with a cross-section of 100 x 150 mm. The parameters studied were the influence of cover depth, compressive and tensile strengths, elastic modulus, and rebar diameter. The concrete's properties were of normal-weight concrete with compressive strength ranging from 20 to 40 MPa. For simplicity, the specimens' tensile strength and elastic modulus were derived from the compressive strength. A fixed-end boundary condition was applied at the top of the beams' cross-section.

Case III was based on Andrade et al. [16] & Molina et al. [17] studies and was adopted to study the influence of the corrosion product (rust's properties) on the simulation results as well as to serve the purpose of validation. The material properties, geometry descriptions and boundary conditions were the same as the said studies [16,17].

2.2.1 Load Analysis

Corrosion is not a standard load in FEM software and is often modelled as internal pressure or radial expansion of the rebar. The applied load in this study was considered as the pressure developed in response to the change in volume of the original steel as a result of a change in its

chemical composition due to corrosion, hence applied as internal pressure. The derivation of the applied load was based on the assumption that there is no diffusion of the corrosion product (rust) into the surrounding concrete and that the rust does not penetrate the corrosion-induced crack before the crack reaches the concrete surface [18].

2.2.2 Derivation of the Applied Pressure

The applied pressure was derived analytically for both uniform and non-uniform corrosion. However, from the comparison based on similar assumptions of one-directional ingress and half of the rebar's section facing the direction of ingress of the corrosion agents, it was observed that uniform corrosion produces a greater volume of steel loss, hence the applied pressure. Accordingly, the uniform corrosion approach was adopted and is presented in this section. It should be noted that the non-uniform corrosion was modelled as an elliptical shape.

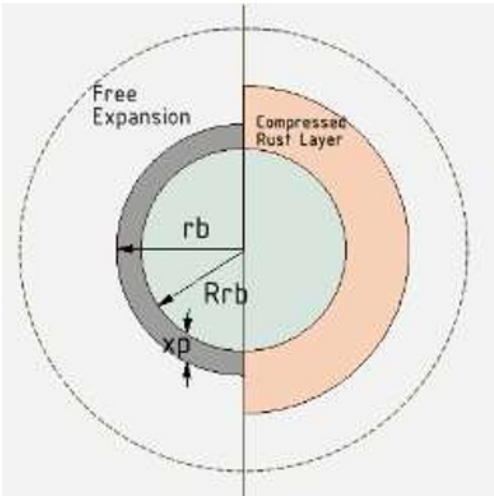

Fig. 4: Schematic of Uniform Corrosion [19]

Consider Figure 4: Let $\boldsymbol{x_p}$ be the radius lost to corrosion (attack penetration), $\boldsymbol{r_b}$ the original radius of the rebar and $\boldsymbol{R_{rb}}$ the residual radius of the rebar. Assuming the expansion to be only in the radial direction, the volume of steel lost to corrosion or being corroded ($\boldsymbol{V_s}$) is:

$$V_s = \pi\left[{r_b}^2 - {R_{rb}}^2\right]h \tag{1}$$

Note: $R_{rb} = r_b - x_p$

The volume of free rust expansion ($\boldsymbol{V_{rust}}$)

$$V_{rust} = V_s \cdot n \tag{2}$$

Where $\boldsymbol{n}$ is the volume expansion ratio. Due to restraint imposed by the surrounding concrete and assuming no diffusion of the corrosion product (rust) into the surrounding concrete, the volume of the free rust expansion will be compressed. Thus, becoming the compressed volume of rust ($\boldsymbol{CV_{rust}}$).

$$CV_{rust} = V_{rust} \cdot \frac{1}{B_{rust}} \tag{3}$$

Where $(\frac{\mathbf{1}}{\boldsymbol{B_{rust}}})$ is the compressibility coefficient of the corrosion product. The inverse of the bulk modulus ($\boldsymbol{B_{rust}}$) of the corrosion product was considered as the volume compressibility coefficient in this analysis. The bulk modulus of the corrosion product is obtained from:

$$B = \frac{E}{3(1-2v)} \tag{4}$$

Where $\boldsymbol{E}$ and $\boldsymbol{v}$ are the elastic modulus and the Poisson's ratio of the rust, respectively. Therefore, the volumetric strain of rust is:

$$\varepsilon_{rust} = \frac{CV_{rust}}{V_{rust}} = \frac{1}{B_{rust}} \tag{5}$$

Note: with the introduction of the compressibility coefficient, the volumetric strain is equal to the radial strain. Thus, from Oh et al.'s [19] proposed formula, the internal pressure (N/mm) acting along the circumference at the steel-concrete interface is:

$$P = k_{rust} \cdot \varepsilon_{rust} \tag{6}$$

Where $\boldsymbol{k_{rust}}$ is the stiffness of the compressed rust layer. The stiffness of the compressed rust layer is the function of its area or thickness and could be obtained with the assumption of a hollow cylinder. However, this approach does not apply to non-uniform corrosion. Therefore, for comparing both derived pressures (uniform and non-uniform), the stiffness was considered in terms of the compressed area multiplied by the elastic modulus of the corrosion product.

$$k_{rust} = \frac{\pi n({r_b}^2 - {R_{rb}}^2)}{B_{rust}} \cdot E_{rust} \tag{7}$$

Where $\boldsymbol{E_{rust}}$ is the elastic modulus of the corrosion product. Consequently, the applied pressure becomes:

$$P = \frac{\pi n({r_b}^2 - {R_{rb}}^2)}{B_{rust}} \cdot E_{rust} \cdot \varepsilon_{rust} \tag{8}$$

For Cases I and II, the applied pressure was calculated using the values of 500 MPa, 0.3, and 4 for the elastic modulus, Poisson's ratio, and volume expansion ratio of the corrosion product (rust), respectively.

3 Main Findings

3.1. Laboratory-based Experiment

Regarding the relationship between the corrosion level and the corrosion-induced crack width, the laboratory investigation showed that this relationship is dependent on the solubility of the corrosion product. It was observed that the largest crack width did not necessarily occur at the maximum cross-section loss along the bars. This effect, as shown in Figure 5, is the consequence of the corrosion product migrating away from the steel-concrete interface and could be attributed to the condition tested (presence of chloride and enough moisture). The presence of chloride increases the solubility of the corrosion products, thus permitting migration and diffusion from the

steel-concrete interface [10]. Therefore, the quantitative description of this relationship was obstructed. However, it was also observed that the cover-diameter ratio influenced the appearance of the corrosion-induced crack, as cracks first appeared on the lowest cover depth for all specimens that cracked.

Fig. 5: Accumulation of Corrosion Product (Control Specimen)

3.2 Numerical Analysis

The results of Case I correlate well with those of the impressed current regarding the influence of cover depth. For all specimens, the simulation results show higher deformation occurring at the lowest cover depth (15 mm). A similar influence of the cover depth was observed with the internal stresses, with the maximum occurring at the 15 mm cover depth. Regarding the specimen's strength, the deformation varies according to the strength of the specimens. The specimen with the lowest strength displayed the highest deformation and vice versa.

From the parametric analysis, the cover depth, tensile strength, and elastic modulus were found to influence the deformation inversely. At a given applied pressure, an increase in any of these parameters decreases the deformation. The influence of the rebar's diameter was evident in the derivation of the applied pressure. When other conditions are constant at a given attack penetration, an increase in the diameter of the rebar will result in a greater section being lost, thus, an increase in the internal pressure, which will also lead to an increase in the deformation and internal stresses.

The impact of the rust's properties on the modelled system, which was studied through Case III, was also observed through the derivation of the applied pressure. The derived applied pressure in Case III was lesser than that of Case II with the same diameter and can be attributed to the properties of the corrosion product adopted by Molina et al. [17], which were the bulk modulus and Poisson's ratio of liquid water. This effect was also reflected in the simulation results, showing smaller deformations.

To summarise the key findings, the applied pressure was found to have a direct dependency on both the volume of steel being oxidised and the properties of the corrosion product and also, directly proportional to the deformations and the resultant stresses.

4 Derivation of the Model

The model's derivation is based on similar assumptions as the applied pressure, including the consideration of uniform corrosion. Although steel corrosion in concrete is never uniform [4,20] nor has a regular shape, such an assumption is necessary for the simplification of the stress analysis [21]. Moreover, the actual non-uniform shape or distribution of the corrosion product around the steel bar is unknown, and the non-uniformity is a unique property. Therefore, the consideration of non-uniform corrosion is also based on assumptions of either elliptical shape or half-ellipse distribution, linearly decreased distribution, or Gaussian distribution, which do not represent the actual non-uniform shape of steel corrosion in concrete.

4.1 Derivation

Assuming concrete to be an isotropic elastic material up to the point of failure in tension.

$$\sigma_{eq} = E_C \varepsilon_{eq} \tag{9}$$

Where $\boldsymbol{\sigma_{eq}}$ is the equivalent stress, $\boldsymbol{E_C}$ the elastic modulus of concrete and $\boldsymbol{\varepsilon_{eq}}$ the equivalent strain. When the equivalent stress exceeds the maximum tensile strength of the concrete, crack initiates, thus, the equivalent strain within the crack zone becomes the strain at cracking ($\boldsymbol{\varepsilon_{cc}}$) [22].

$$\sigma_{eq} = E_C \varepsilon_{cc} \tag{10}$$

The equivalent strain at cracking is proportional to the crack width with the assumption that no interlocking exists, hence, the shear goes to zero [22]. From Bangash [22], the proportionality constant is given as the volume containing the crack divided by the area of the crack. However, from the laboratory investigation and simulation results, it was shown that the appearance of cracks and deformations, respectively, strongly depend on the cover-diameter ratio. Therefore, the cover-diameter ratio was considered the proportionality constant in this analysis and is expressed in Equation – 11.

$$w = \frac{c}{D} \varepsilon_{cc} \tag{11}$$

Where $\boldsymbol{w}$ is the width of the crack, $\boldsymbol{c}$ the cover depth and $\boldsymbol{D}$ the rebar diameter. Making the strain at cracking ($\boldsymbol{\varepsilon_{cc}}$) the subject, Equation – 11 becomes:

$$\varepsilon_{cc} = \frac{D}{c} w \tag{12}$$

Substituting Equation – 12 into Equation – 10 yields:

$$\sigma_{eq} = \frac{D}{c} E_C w \tag{13}$$

Note: the simulation results showed that the applied pressure (internal pressure arising as the result of corrosion) is directly proportional to the equivalent stress.

$$P \approx \sigma_{eq} \quad (14)$$

Also, from the simulations, the proportionality constant was observed to be closely related for all cases. The maximum value of 2.05 was adopted in this derivation.

$$P = 2.05\sigma_{eq}$$

$$P = 2.05\left[\frac{D}{c} \cdot E_C \cdot w\right] \quad (15)$$

Recall from Equation – 8 the applied pressure (P) is:

$$P = \frac{\pi n({r_b}^2 - {R_{rb}}^2)}{B_{rust}} \cdot E_{rust} \cdot \varepsilon_{rust}$$

Expressing $\boldsymbol{\varepsilon_{rust}}$ in terms of the compressibility coefficient of the corrosion product, the applied pressure becomes:

$$P = \frac{\pi n({r_b}^2 - {R_{rb}}^2)}{B_{rust}} \cdot E_{rust} \cdot \frac{1}{B_{rust}} \quad (16)$$

Simplifying yields:

$$P = \frac{\pi n({r_b}^2 - {R_{rb}}^2) \cdot E_{rust}}{{B_{rust}}^2} \quad (17)$$

Also, expressing $\boldsymbol{B_{rust}}$ in terms of the rust's elastic modulus and Poisson's ratio, and simplifying yields:

$$P = \frac{\pi n({r_b}^2 - {R_{rb}}^2) \cdot [3(1-2v)]^2}{E_{rust}} \quad (18)$$

There is consensus among researchers regarding the volume expansion ratio and Poisson's ratio of corrosion products than its elastic modulus. The elastic modulus of corrosion products reported in the literature varies greatly and depends on the environment. However, some researchers have estimated the elastic modulus to be in the range of 0.1 to 0.5 GPa, which has been verified by Zhao and Jin [21]. In this regard, the influence of the rust's elastic modulus in the above equation must be mitigated. The mitigation was achieved by fixing the value to 1 GPa and keeping it constant since the value adopted in calculating the applied pressure was 500 MPa (0.5 GPa). Likewise, the Poisson's ratio of rust is usually considered the same as that of the steel being oxidised, hence 0.3 was adopted. This approach allowed the proposed relationship to be dependent on the volume expansion ratio of the corrosion product. It should be noted that the corrosion-induced crack appears because of the rust expansion. Thus, substituting 1 GPa and 0.3 for $\boldsymbol{E_{rust}}$ and $\boldsymbol{v}$, respectively in Equation – 18 yields:

$$P = 1.44\pi n({r_b}^2 - {R_{rb}}^2)GPa^{-1} \quad (19)$$

Substituting for P into Equation – 15 yields:

$$1.44\pi n({r_b}^2 - {R_{rb}}^2)GPa^{-1} = 2.05\left[\frac{D}{c} \cdot E_C \cdot w\right] \quad (20)$$

Simplifying, the residual radius becomes:

$$R_{rb} = \sqrt{{r_b}^2 - \frac{2.05\left[\frac{D}{c} \cdot E_C \cdot w\right]GPa}{1.44\pi n}} \quad (21)$$

At this stage of the derivation, empirical reasoning is employed to modify Equation – 21, which enables the equation to be solved as well as to obtain the desired unit. The modification involves the introduction of "mm" and "GPa^2" on the right-hand side of Equation – 21, in the numerator and denominator, respectively. Equation. – 21, therefore, becomes:

$$R_{rb} = \sqrt{{r_b}^2 - \frac{2.05mm\left[\frac{D}{c} \cdot E_C \cdot w\right]GPa}{1.44\pi nGPa^2}} \quad (22)$$

Equation – 22 presents an expression from which the residual radius can be estimated. Where $\boldsymbol{R_{rb}}$ is the residual radius of the rebar (mm), $\boldsymbol{r_b}$ the original radius of the rebar (mm), $\boldsymbol{D}$ the rebar diameter (mm), $\boldsymbol{c}$ the cover depth (mm), $\boldsymbol{E_c}$ the concrete's elastic modulus (GPa), $\boldsymbol{w}$ the corrosion-induced crack width (mm) and $\boldsymbol{n}$ the volume expansion ratio of the corrosion product.

The derived model requires input parameters that are easily obtainable both in the laboratory and the field. Apart from the volume expansion ratio of the corrosion product, all the required input parameters can be obtained by non-destructive testing. In the above derivation, the residual section or remaining cross-section of the corroding bar is expressed in terms of the residual radius. With this approach, the model is applicable to both generalised and localised corrosion and, accommodates multi-directional ingress of corrosion agents, thus, improving the versatility and accuracy.

5 Validation of the Derived Model

The derived model was tested against data from the laboratory investigation and experimental and analytical data from the literature. The experimental data considered were those of Andrade et al. [16] and Vidal et al. [15], while the analytical data was that of Chen and Leung [23]. In the validation, the value of the volume expansion ratio of the corrosion product is the same as the applied pressure.

5.1. Laboratory Investigation Data

The validation of the derived model against data from the laboratory investigation showed the highest deviation, with average percentage errors of 10.8, 9.1, 8.7 and 6.6 % for the four specimens that cracked. The control specimen, which was made of 100% rapid hardening Portland cement, exhibited the maximum percentage error. The deviation is attributed to the migration of the corrosion product away from the steel-concrete interface and accumulating at the surface of the ponding basin, as was discussed in Section 3.1. The migration of the corrosion product away from the steel-concrete interface not only reduces the pressure exerted on the surrounding concrete, which influences the corrosion-induced crack width but also distorts the relationship between the section loss and the corrosion-induced crack width. It is worth noting that the derivation of the model did not consider the effect of corrosion product migrating from the steel-concrete interface, hence, could serve as a limitation.

Details of the model validation against data of the control specimen are presented in Table 1. The averages of the crack width and cross-section loss were used in the validation. The crack widths were measured at four points along the rebar's exposed length with the aided of Elcometer crack microscope for crack widths less than 1.8 mm and with a crack ruler for those greater than 1.8 mm.

For the cross-section loss, a vernier calliper with an accuracy of 0.01 mm was used to measure the residual diameter of the rebar. The average residual diameter consisted of the diameter measured across the most affected sections and those corresponding to the map-out crack pattern as shown in Figure 6, which displays the map-out crack pattern of the control specimen.

Table 1: Model validation against the laboratory data (Control Specimen).

Control Specimen										
$Bars$	D (mm)	c (mm)	$\frac{D}{c}$	r_b (mm)	w (mm)	E_c (GPa)	x_p (mm)	R_{rb} (mm)	***Based on Derived Model***	
									$\boldsymbol{R_{rb}}$	$\boldsymbol{Error}(\%)$
Bar-1	10	15	0.67	5	0.85	31.67	0.86	4.14	4.79	15.83%
Bar-2	10	15	0.67	5	1.23	31.67	0.80	4.21	4.70	11.72%
Bar-3	10	15	0.67	5	0.40	31.67	0.50	4.51	4.90	8.84%
Bar-4	10	30	0.33	5	0.10	31.67	0.57	4.43	4.99	12.60%
Bar-5	10	30	0.33	5	1.53	31.67	0.81	4.19	4.81	14.83%
Bar-6	10	30	0.33	5	0.85	31.67	0.06	4.94	4.90	0.82%
									Ave:	**10.8%**

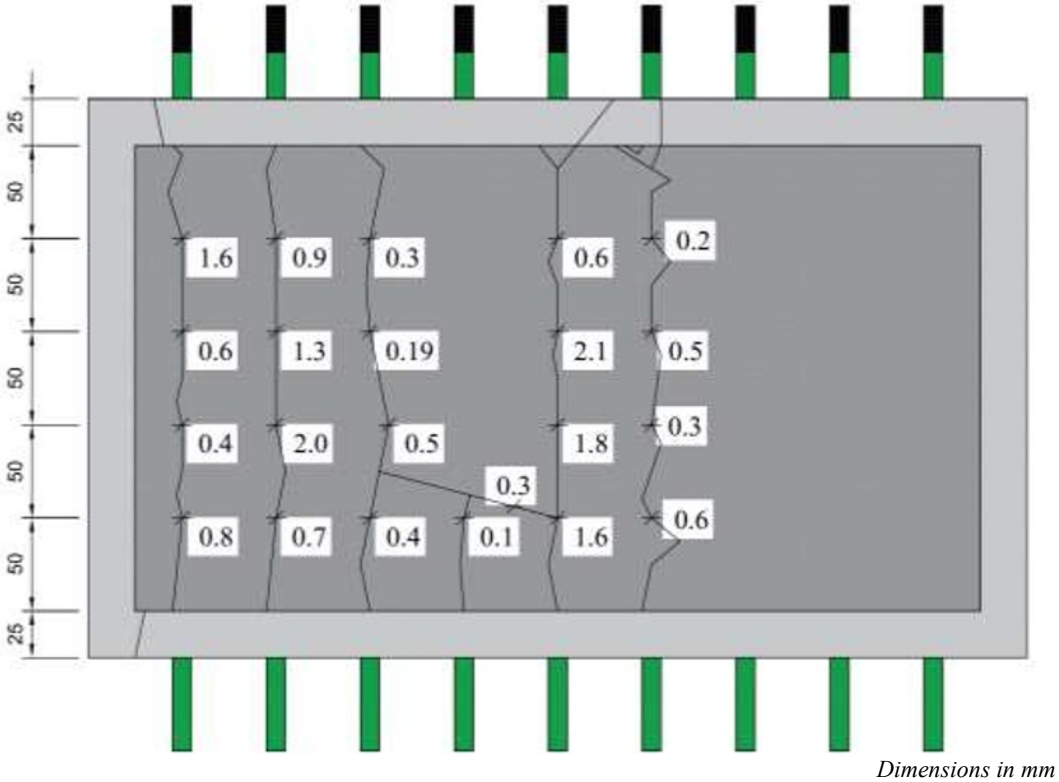

Dimensions in mm

Figure 6: Crack Pattern of the Control Specimen.

5.2. Andrade et al.'s (1993) Data

Andrade et al.'s [16] data is based on an accelerated corrosion test, which consisted of four reinforced concrete beams (specimen I, II, III and IV). The dimensions of the specimens were 38 x 15 x 15 cm. Each specimen contained a single rebar with a diameter of 16 mm, and a concrete cover depth of either 2 or 3 cm. Details of the material properties can be found in Andrade et al. [16] & Molina et al. [17]. The applied currents were 100 and 10 $\mu A/cm^2$ for specimens I, II, III and IV, respectively, with the assumption that 100% of the current applied was consumed in the corrosion process. It is worth noting that the authors calculated the radius loss (attack penetration) based on the above assumption. The data used for this validation are found in Figure 8 – Figure 11 of Andrade et al. [16]. The validation of the derived model showed a good correlation with an average percentage error of 0.35, 0.43, 0.25 and 0.12 %, for specimens I, II, III and IV, respectively.

5.3. Vidal et al.'s (2004) Data

Vidal et al.'s [15] experimental data were collected from two reinforced concrete beams that had corroded naturally in a simulated chloride environment under loading. The beams considered had the dimension of 3000 x 150 x 280 mm, an average 28-day compressive strength of 45 MPa and an elastic modulus of 32 GPa. The beams were labelled Beam A and Beam B and contained rebars of 16- and 12-mm diameter at cover depths of 48 and 16 mm, respectively. The Data used in this validation was collected from Figure 10 of Vidal et al. [15], with the aid of WebPlotDigitizer software. The validation revealed an average percentage error of 0.42 and 1.52 % for both tensile and compressive reinforcement in Beam A, and Beam B, respectively.

5.4. Chen and Leung's (2013) Data

Chen and Leung's [23] study is based on a numerical model of corrosion-induced cracking and chloride diffusion process. Two specimens with a cross-section of 150 x 150 mm, containing a single rebar of 20 mm diameter were considered. Each specimen was analysed based on uniform and non-uniform corrosion. The specimens were assigned an elastic modulus of 36 GPa and concrete cover depth of 20 and 40 mm, respectively. The data used in this validation are presented in Table 2 and Table 3 of Chen and Leung [23] and were obtained from finite element analysis of various penetration depths, which give the corresponding crack widths. For the non-uniform corrosion data, which has a range of attack penetrations (corroded depths), an average value was considered. The validation of the derived model against Chen and Leung's data showed the best correlation with an average percentage error of 0.03 and 0.05% for uniform and non-uniform corrosion at 20 mm cover depth, respectively, and 0.19 and 0.18% for uniform and non-uniform corrosion at 40 mm cover depth. The best-fitting is attributed to the absence of the migration or diffusion effect of the corrosion product. Table 2 and Table 3 display details of the model validation against Chen and Leung's uniform and non-uniform corrosion data at 20 mm cover depth, respectively.

Table 2: Model validation against Chen and Leung's Data (Uniform Corrosion).

Uniform Corrosion @ Cover depth of 20 mm									
D (mm)	c (mm)	$\frac{D}{c}$	r_b (mm)	w (mm)	E_c (GPa)	x_p (mm)	R_{rb} (mm)	***Based on Derived Model***	
								$\boldsymbol{R_{rb}}$	***Error***(%)
20	20	1	10	0.099	36	0.016	9.9840	9.9798	0.04%
20	20	1	10	0.138	36	0.024	9.9760	9.9718	0.04%
20	20	1	10	0.165	36	0.032	9.9680	9.9663	0.02%
20	20	1	10	0.225	36	0.044	9.9560	9.9540	0.02%
20	20	1	10	0.280	36	0.056	9.9440	9.9427	0.01%
20	20	1	10	0.338	36	0.064	9.9360	9.9308	0.05%
20	20	1	10	0.366	36	0.072	9.9280	9.9250	0.03%
20	20	1	10	0.406	36	0.080	9.9200	9.9168	0.03%
20	20	1	10	0.463	36	0.092	9.9080	9.9051	0.03%
20	20	1	10	0.497	36	0.100	9.9000	9.8981	0.02%
								Ave:	**0.03%**

Table 3: Model validation against Chen and Leung's Data (Non-uniform Corrosion).

Non-uniform Corrosion @ Cover depth of 20 mm									
D (mm)	c (mm)	$\frac{D}{c}$	r_b (mm)	w (mm)	E_c (GPa)	x_p (mm)	R_{rb} (mm)	***Based on Derived Model***	
								$\boldsymbol{R_{rb}}$	***Error***(%)
20	20	1	10	0.137	36	0.024	9.9760	9.9720	0.04%
20	20	1	10	0.191	36	0.036	9.9640	9.9610	0.03%
20	20	1	10	0.257	36	0.048	9.9520	9.9474	0.05%
20	20	1	10	0.307	36	0.060	9.9400	9.9372	0.03%
20	20	1	10	0.385	36	0.072	9.9280	9.9211	0.07%
20	20	1	10	0.436	36	0.084	9.9160	9.9106	0.05%
								Ave:	**0.05**

6 Concluding Remarks

This paper presents a model for quantifying corrosion damage in reinforced concrete structures in terms of the residual cross-section of the corroding bar. The derived model applies to structures in service and requires simple input parameters that are also obtainable by non-destructive testing. The decision to express the corrosion damage in terms of cross-section loss stems from the fact that the principal effect of corrosion is the cross-section loss of the steel reinforcement. It is expected that the proposed model will assist engineers in deciding when to recommend appropriate repairs for corrosion-damaged concrete structures based on an informed assessment of the residual cross-section of the corroding bar. The model was tested against data from the laboratory investigation and other experimental and analytical data from the literature, and the results showed a good correlation. However, the proposed model is not without limitations, which result from some variables not considered in the analyses, especially the diffusion effect of the corrosion product and partially, due to some of the assumptions employed in the derivation.

References

1. R.M. Ferreira, Probability-Based Durability Analysis of Concrete Structures in Marine Environment, (2004).
2. J. Broomfield, Introduction, In: *Corrosion of Steel in Concrete: Understanding, Investigation and Repair*, Crc Press, (2003).
3. C. Andrade, A. Cesetti, G. Mancini, F. Tondolo, Estimating Corrosion Attack in Reinforced Concrete by Means of Crack Opening, *Struct. Concr.* **17** (2016) 533–540.
4. G. Malumbela, M. Alexander, P. Moyo, Model for Cover Cracking of RC Beams Due to Partial Surface Steel Corrosion, *Constr. Build. Mater.* **25** (2011) 987–991.
5. I. Khan, R. François, A. Castel, Prediction of Reinforcement Corrosion Using Corrosion Induced Cracks Width in Corroded Reinforced Concrete Beams, *Cem. Concr. Res.* **56** (2014) 84–96.
6. T. Dyer, Corrosion of Steel Reinforcement in Concrete, In: *Concrete Durability*, Crc Press, (2014).
7. S.O. Nwaubani, A. Katsanos, Effect of Alternative De-Icers on the Corrosion Resistance of Reinforced Concrete Bridges and Highway Structures, In: *Developments in Corrosion Protection*, InTech, (2014).
8. R. Zhang, A. Castel, R. François, Concrete Cover Cracking with Reinforcement Corrosion of RC Beam during Chloride-Induced Corrosion Process, *Cem. Concr. Res.* **40** (2010) 415–425.
9. L. Yu, R. François, V.H. Dang, V. L'Hostis, R. Gagné, Distribution of Corrosion and Pitting Factor of Steel in Corroded RC Beams, *Constr. Build. Mater.* **95** (2015) 384–392.
10. U.M. Angst, Challenges and Opportunities in Corrosion of Steel in Concrete, *Mater. Struct.* **51** (2018).
11. C. Andrade, M.C. Alonso, J.A. Gonzalez, An Initial Effort to Use the Corrosion Rate Measurements for Estimating Rebar Durability, In: *Corrosion Rates of Steel in Concrete, ASTM Symposium*, (1988).
12. C. Andrade, C. Alonso, J.A. Gonzalez, J. Rodriguez, Remaining Service Life of Corroding Structures, In: *Durability of Structures. IABSE Symposium*, (1989).
13. J. Rodriguez, L.M. Ortega, J. Casal, J.M. Diez, Corrosion of Reinforcement and Service Life of Concrete Structures, *Durab. Build. Mater. Compon.* **7** (1996) 117–126.
14. C. Alonso, C. Andrade, J. Rodriguez, J.M. Diez, Factors Controlling Cracking of Concrete Affected by Reinforcement Corrosion, *Mater. Struct.* **31** (1998) 435–441.
15. T. Vidal, A. Castel, R. François, Analyzing Crack Width to Predict Corrosion in Reinforced Concrete, *Cem. Concr. Res.* **34** (2004) 165–174.
16. C. Andrade, C. Alonso, F.J. Molina, Cover Cracking as a Function of Bar Corrosion: Part I-Experimental Test, *Mater. Struct.* **26** (1993) 453–464.
17. F.J. Molina, C. Alonso, C. Andrade, Cover Cracking as a Function of Rebar Corrosion: Part 2—Numerical Model, *Mater. Struct.* **26** (1993) 532–548.
18. Y. Zhao, J. Yu, B. Hu, W. Jin, Crack Shape and Rust Distribution in Corrosion-Induced Cracking Concrete, *Corros. Sci.* **55** (2012) 385–393.
19. B.H. Oh, K.H. Kim, B.S. Jang, J.S. Kim, S.Y. Jang, Realistic Model for Corrosion-Induced Cracking in Reinforced Concrete Structures, (2007).
20. S. Muthulingam, B.N. Rao, Non-Uniform Corrosion States of Rebar in Concrete under Chloride Environment, *Corros. Sci.* **93** (2015) 267–282.
21. Y. Zhao, W. Jin, Steel Corrosion-Induced Concrete Cracking, Butterworth-Heinemann, (2016).
22. M.Y.H. Bangash, Numerical Modelling of Concrete Strength and Failure, In: *Concrete and Concrete Structures: Numerical Modelling and Applications*, Elsevier Applied Science, (1989).
23. E. Chen, C.K.Y. Leung, Numerical Modelling of Non-Uniform Steel Corrosion Development and Its Mechanical Influences on Reinforced Concrete Structures, In: *VIII International Conference on Fracture Mechanics of Concrete and Concrete Structures (FraMCoS-8)*, (2013).